Isonitrile Binding to a Site-Differentiated Synthetic Analogue of Biological [4Fe-4S] Clusters: Equilibria, Magnetic Interactions and the Spin-Isolated [3Fe-4S] Cluster Fragment, and the Structure of a Low-Spin Iron(II) Subsite

J. A. Weigel,[1a] K. K. P. Srivastava,[1b] E. P. Day,[1b] E. Münck,*[,1b] and R. H. Holm*[,1a]

Contribution from the Department of Chemistry, Harvard University, Cambridge, Massachusetts 02138, and Gray Freshwater Biological Institute, University of Minnesota, Navarre, Minnesota 55392. *Received March 22, 1990*

Abstract: The cubane-type cluster $[Fe_4S_4(LS_3)Cl]^{2-}$ [**3**, LS_3 = tris[(4,6-dimethyl-3-mercaptophenyl)thio]-2,4,6-tris(*p*-tolylthio)benzene(3-)] contains iron subsites differentiated in the ratio 3:1. Cluster **3** undergoes substitution reactions at the unique subsite with stoichiometric cyanide and excess isonitrile in acetonitrile solution to afford $[Fe_4S_4(LS_3)(CN)]^{2-}$ (**4**) and $[Fe_4S_4(LS_3)(RNC)_3]^{1-}$ [R = Me (**5**), Et, *t*-Bu (**7**), C_6H_{11}, and 2,6-$Me_2C_6H_3$ (**9**)], respectively. The reaction products were identified by their characteristic isotropically shifted ^1H NMR spectra, which are consistent with trigonal symmetry. Equilibrium constants for the binding of three RNC ligands range from 380 (**5**) to 4.9×10^5 M^{-2} (**9**) at 297 K. The reactions have large negative entropy changes and are moderately exothermic: ΔH = -23 (**5**) and -27 (**7**) kcal/mol. Mössbauer spectroscopic and magnetic susceptibility studies of (Ph_4P)[**7**] demonstrate the existence of a low-spin Fe(II) subsite, assigned to the trigonal $Fe(RNC)_3$ group, and a spin-isolated $[Fe_3S_4]^0$ cluster fragment. The latter is shown to have the same ground-state electronic structure as singly reduced 3Fe clusters of proteins: an $S = 2$ state derived from a high-spin Fe^{3+} subsite ($S = {}^5/_2$) and a pair of ferromagnetically coupled, electronically delocalized Fe atoms ($Fe^{2.5+}$, $S = {}^9/_2$). Given the common spin ground state, the impressive similarity among zero-field-splitting parameters and magnetic hyperfine tensors, and the different structural environments, it is highly probable that the spin-coupled $S = 2$ ground state is an intrinsic property of the $[Fe_3S_4]^0$ core. This state explains the much larger ^1H isotropic shifts of the isonitrile clusters compared to **4**. The cyanide cluster binds only one strong-field ligand and retains the conventional $S = 0$ ground state of $[Fe_4S_4]^{2+}$ clusters such as **3**. The failure to detect clusters with one or two RNC ligands indicates that for the stepwise formation constants, $K_{2-3} \gg K_{1-2}$, K_{0-1}. This situation is brought about by the ligand field stabilization energy of low-spin Fe(II), whose formation is induced by the binding of three strong-field ligands. The reaction of $[Fe_4S_4Cl_4]^{2-}$ with excess *t*-BuNC in THF gives $[Fe_4S_4Cl_2(t\text{-BuNC})_6]$ in 60% yield. This compound crystallizes in monoclinic space group $C2/c$ with a = 11.834 (2) Å, b = 21.195 (3) Å, c = 18.523 (3) Å, β = 93.64 (1)°, and $Z = 4$. It contains the cubane $[Fe_4S_4]^{2+}$ core, which has two tetrahedral FeS_3Cl subsites of standard dimensions [Fe-Fe = 2.741 (3) Å] and two trigonal-octahedral $FeS_3(t\text{-BuNC})_3$ subsites whose Mössbauer properties are nearly identical with those of the unique subsite of **7**. The six-coordinate subsites are separated from each other by 3.444 (3) Å and from the tetrahedral sites by 2.994 (3) Å. It is probable that the unique site in $[Fe_4S_4(LS_3)(RNC)_3]^{1-}$ has a closely similar stereochemistry and is separated from the Fe atoms of the spin-isolated Fe_3S_4 cluster fragment by >3 Å. The structure of the cluster is analyzed and compared with that of the cubane $[Fe_4S_4(CO)_{12}]$, which contains low-spin $Fe^{II}S_3(CO)_3$ subsites.

Introduction

We have previously reported the preparation of the trithiol $L(SH)_3$ (**1**) and its application to the synthesis of the generalized cubane-type clusters $[Fe_4S_4(LS_3)L']^z$ (**2**) in which the Fe subsites are differentiated in a ratio of 3:1.[2,3] Formulas of **1** and **2** are shown in Figure 1. In these clusters, the three coordinating arms of the ligand bind the Fe_4S_4 core on one side of the central benzene ring and the three buttressing legs are disposed on the other side of this ring. A conformational analysis of the free ligand indicates that its principal conformers are predisposed to capture a cubane cluster by binding at three subsites.[3] It has been possible to place at the unique subsite, often by substitution of chloride in $[Fe_4S_4(LS_3)Cl]^{2-}$ (**3**), a considerable variety of mono-, bi-, and tridentate ligands.[2-7] The ^1H NMR spectra of such clusters, all of which contain the $[Fe_4S_4]^{2+}$ core, are consistent with an $S = 0$ ground state and trigonal symmetry. The isotropic components of the chemical shifts, which are responsible for the highly resolved spectra usually observed, arise from a population of low-lying paramagnetic states.[8]

Access to site-differentiated clusters facilitates the investigation of recently recognized, subsite-specific reactivity, structural, and electronic aspects of native clusters.[4] Appropriately derivatized forms **2** serve as synthetic analogues. By use of substitution reactions, we have prepared bridged double-cubane clusters and examined the coupling between subclusters in redox reactions as dependent upon the distance between them.[5] A further application of site-differentiated clusters is the determination of the influence of different ligands at the unique subsite on the relative stabilities of oxidation states, and charge distribution and the magnitude of spin coupling within the $[Fe_4S_4]^{2+}$ core. Recently, we have shown that redox potentials and charge distributions of clusters can be significantly modulated by alteration of the ligand at the unique subsite. In particular, dithiolate ligands are notably effective in causing large negative shifts of redox potentials.[6]

Among the ligands that have been placed at the unique subsite of the cluster **2** are classical anionic π-donors, several π-acceptors including CN^- and $C_5H_5^-$, and the neutral tridentate 1,4,7-triazacyclononane. As noted above, these clusters have a diamagnetic ground state. However, the only other neutral ligands thus far found to bind to the cluster, alkyl and aryl isonitriles, behave very differently and do not preserve this ground state. We provide here a full account of the site-specific substitution reactions of isonitriles with $[Fe_4S_4(LS_3)Cl]^{2-}$, the electronic structure of the resultant cluster, and the stereochemical consequences of binding these

(1) (a) Harvard University. (b) University of Minnesota.
(2) Stack, T. D. P.; Holm, R. H. *J. Am. Chem. Soc.* **1988**, *110*, 2484.
(3) Stack, T. D. P.; Weigel, J. A.; Holm, R. H. *Inorg. Chem.*, in press.
(4) Holm, R. H.; Ciurli, S.; Weigel, J. A. *Prog. Inorg. Chem.*, in press.
(5) Stack, T. D. P.; Carney, M. J.; Holm, R. H. *J. Am. Chem. Soc.* **1989**, *111*, 1670.
(6) Ciurli, S.; Carrié, M.; Weigel, J. A.; Carney, M. J.; Stack, T. D. P.; Papaefthymiou, G. C.; Holm, R. H. *J. Am. Chem. Soc.* **1990**, *112*, 2654.
(7) Weigel, J. A.; Holm, R. H., results to be published.
(8) Reynolds, J. G.; Laskowski, E. J.; Holm, R. H. *J. Am. Chem. Soc.* **1978**, *100*, 5315.

0002-7863/90/1512-8015$02.50/0

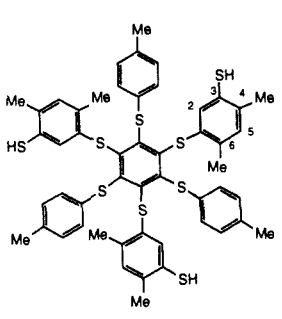

1

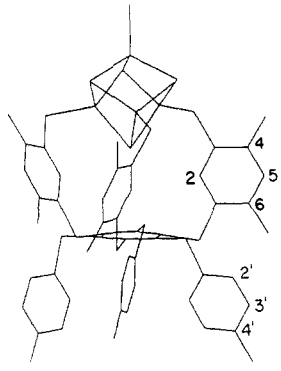

2

Figure 1. Formulas of tridentate ligand $L(SH)_3$ (**1**) and the generalized site-differentiated clusters $[Fe_4S_4(LS_3)L']^z$ (**2**) adapted from the X-ray structure of $[Fe_4Se_4(LS_3)Cl]^{2-}$.[3] Formula **2** illustrates the trigonal conformation in solution; the ligand numbering scheme is indicated.

strong-field ligands. Certain leading results of this study have been briefly reported.[9]

Experimental Section

Preparation of Compounds. The compounds $(Ph_4P)_2[Fe_4S_4(LS_3)Cl]$,[2,3] $(Ph_4P)_2[Fe_4S_4Cl_4]$,[10] MeNC,[11] and EtNC[12] were prepared by published methods. All other compounds were commercial samples and were used as received. In the preparations of cluster compounds, all operations were carried out under a pure dinitrogen atmosphere with use of degassed solvents.

$(Ph_4P)[Fe_4S_4(LS_3)(t\text{-BuNC})_3]$ ((Ph_4P)[7]). To a solution of 69.6 mg (34.6 μmol) of $(Ph_4P)_2[Fe_4S_4(LS_3)Cl]$ in 50 mL of acetonitrile was added 3.80 mg (34.6 μmol) of $NaBF_4$. This solution was treated with 40 μL (346 μmol) of *t*-BuNC, stirred for 15 min, and filtered through a Celite plug to remove NaCl. Removal of solvent from the filtrate in vacuum afforded the product as a black air-sensitive solid. ^1H NMR (CD_3CN, 297 K): δ 0.38 (*t*-Bu), 2.57 (4'-Me), 6.47 (3'-H), 8.49 (2'-H), 10.98 (4-Me), 14.94 (6-Me), 16.52 (5-H). Absorption spectrum (CH_2Cl_2): λ_{max}, nm (ϵ_M) 306 (sh, 43 200), 500 (sh, 10 100). IR (KBr): ν_{NC} 2123, 2153 cm^{-1}.

$[Fe_4S_4Cl_2(t\text{-BuNC})_6]$ (10). To a suspension of 0.500 g (0.427 mmol) of $(Ph_4P)_2[Fe_4S_4Cl_4]$ in 50 mL of THF was added 964 μL (8.53 mmol) of *t*-BuNC. The mixture was heated to reflux and stirred for 2 h, during which time the solution took on a dark purple color and a white solid precipitated. The mixture was allowed to stand at room temperature for 12 h and was filtered; 50 mL of ether was added to the filtrate. Storage at −20 °C overnight resulted in the separation of a dark purple crystalline solid. This material was collected by filtration, washed with ether, and dried in vacuum to afford 235 mg (60%) of product. An analytical sample was obtained by recrystallization from THF/ether. Anal. Calcd for $C_{30}H_{54}Cl_2Fe_4N_6S_4$: C, 39.11; H, 5.91; Cl, 7.70; Fe, 24.25; N, 9.12. Found: C, 39.21; H, 5.82; Cl, 7.92; Fe, 24.00; N, 9.09. ^1H NMR (CD_2Cl_2): δ 1.39 (2), 1.65 (1). Absorption spectrum (CH_2Cl_2): λ_{max}, nm (ϵ_M) 532 (3780). IR (KBr): ν_{NC} 2114, 2145 cm^{-1}.

$[Fe_4S_4(LS_3)(RNC)_3]^{1-}$ (5, 6, 8, and 9). These clusters were generated in solution by the reaction of **3** with ca. 10 equiv of RNC, but were not isolated. Their formation was demonstrated by their ^1H NMR spectra in acetonitrile (297 K), which gave no detectable signals other than those of the clusters and excess isonitrile. Chemical shifts (δ) of clusters are given in the order R = Me (**5**), Et (**6**), C_6H_{11} (**8**), and 2,6-$Me_2C_6H_3$ (**9**): 4-Me, 10.87, 10.89, 10.88, 11.51; 5-H, 16.62, 16.55, 16.47, 16.83; 6-Me, 15.06, 14.97, 14.77, 15.15; 2'-H, 8.54, 8.55, 8.58, 8.97; 3'-H, 6.56, 6.53, 6.51, 6.59; 4'-Me, 2.59, 2.59, 2.59, 2.67. R: −4.11; −3.16 (CH_2), 1.28 (Me); −2.04 (CH); 0.87 (Me), 6.31 (3,5-H). The remaining signals of **8** and **9** were obscured by other resonances or could not be assigned with certainty.

Equilibrium Constants. Values of K_{eq} for the reaction of cluster **3** with various isonitriles were determined at 297 K in CD_3CN solutions. The concentrations of **3** (initially ca. 1 mM), free RNC, and products **5–9** were obtained by monitoring ^1H NMR signal intensities. For each reaction, spectra of at least eight equilibrium solutions were recorded and equilibrium constants were calculated; the mean value of these determinations is reported. For two reactions, this procedure was extended to lower temperatures in order to determine ΔH and ΔS from the temperature dependence of K_{eq}.

Table I. Crystallographic Data for $[Fe_4S_4Cl_2(t\text{-BuNC})_6]$

formula	$C_{30}H_{54}Cl_2Fe_4N_6S_4$
mol wt	921.44
a, Å	11.834 (2)
b, Å	21.195 (3)
c, Å	18.523 (3)
β, deg	93.64 (1)
space group	*C*2/*c*
V, Å^3	4638 (1)
Z	4
ρ_{calc} (ρ_{obs}),[a] g/cm^3	1.32 (1.33)
T, K	298
radiation	Mo Kα (λ = 0.71069)
μ, cm^{-1}	15.43
R,[b] %	6.77
R_w,[c] %	8.64[d]

[a] Determined by the neutral buoyancy in CCl_4/hexane. [b] $R = \sum||F_o| - |F_c||/\sum|F_o|$. [c] $R_w = \sum[w^{1/2}(||F_o| - |F_c||)]/\sum[w^{1/2}|F_o|]$. [d] Weighting scheme for least-squares refinement: $w^{-1} = \sigma^2(F) + 0.0110(F^2)$.

Collection and Reduction of X-ray Data. Dark purple crystals of $[Fe_4S_4Cl_2(t\text{-BuNC})_6]$ were grown by layering ether onto a THF solution and allowing the mixture to stand at room temperature. Single crystals were mounted with Apiezon grease in glass capillaries under a dinitrogen atmosphere, and the capillaries were flame-sealed. Data collection was performed using a Nicolet P3F four-circle diffractometer equipped with a Mo X-ray tube and a graphite monochromator. The orientation matrix and unit cell parameters were determined by a least-squares fit of the angular coordinates of 50 machine-centered reflections having $15° \le 2\theta \le 29°$. Crystal parameters are included in Table I. Three check reflections monitored every 100 reflections exhibited no significant decay over the course of the data collection. Lorentz and polarization corrections were applied with XDISK from the SHELXTL program package (Nicolet XRD Corp., Madison, WI 53711), and an empirical absorption correction (XEMP) was applied. The compound crystallizes in the monoclinic system; the systematic absences *hkl*, 0*kl*, *hk*0 ($h + k \neq 2n$), *h*0*l* (h, $l \neq 2n$), *h*00 ($h \neq 2n$), 0*k*0 ($k \neq 2n$), and 00*l* ($l \neq 2n$) are consistent with space groups *Cc* and *C*2/*c*. Simple *E* statistics favored the choice of a centrosymmetric cell, which was confirmed by successful solution and refinement of the structure to low error indices.

Structure Solution and Refinement. Atom scattering factors were taken from the tabulation of Cromer and Waber.[13] The Fe, S, and Cl atoms were located by direct methods. The remaining non-hydrogen atoms were located in successive difference Fourier maps, and were refined by using SHELXTL. Twofold symmetry is crystallographically imposed on the cluster molecule. All non-hydrogen atoms were refined anisotropically except for the carbon atoms of the *tert*-butyl groups. Owing to extensive disorder, these groups were refined as rigid rotors with fixed C–C bond distances of 1.50 Å. In the last cycle of refinement, all parameters shifted by <1% of their esd, and the highest residual peak in the final difference map (ca. 2 e/Å^2) was located in the vicinity of the Fe(1) atom. Final *R* values are given in Table I.[14]

Other Physical Measurements. All measurements were performed under strictly anaerobic conditions. ^1H NMR spectra were recorded on a Bruker AM-500 spectrometer. Electrochemical measurements were recorded in dichloromethane solutions using standard PAR instrumentation, a Pt working electrode, and 0.1 M $Bu_4N(PF_6)$ supporting electrolyte. Potentials are determined vs an aqueous SCE; under the experimental conditions, $E_{1/2}(Fc^+/Fc) = +0.470$ V. In controlled-potential coulometry the working electrode was a Pt mesh. Mössbauer spectroscopic measurements were made utilizing the equipment and techniques described earlier.[15] Isomer shifts are quoted relative to Fe metal at room temperature.

Magnetic measurements were performed on a Quantum Design susceptometer modified by the manufacturer to produce a continuous gas

(9) Weigel, J. A.; Holm, R. H.; Surerus, K. K.; Münck, E. *J. Am. Chem. Soc.* **1989**, *111*, 9246.
(10) Wong, G. B.; Bobrik, M. A.; Holm, R. H. *Inorg. Chem.* **1978**, *17*, 578.
(11) Casanova, J., Jr.; Schuster, R. E.; Werner, N. D. *J. Chem. Soc.* **1963**, 4280.
(12) Weber, W. P.; Gokel, G. W.; Ugi, I. *Angew. Chem., Int. Ed. Engl.* **1972**, *11*, 530.
(13) Cromer, D. T.; Waber, J. T. *International Tables for X-ray Crystallography*; Kynoch Press: Birmingham, England, 1974, Vol. IV.
(14) See the paragraph at the end of this article concerning supplementary material available.
(15) Zimmermann, R.; Münck, E.; Brill, W. J.; Shah, V. K.; Henzl, M. T.; Rawlings, J.; Orme-Johnson, W. H. *Biochim. Biophys. Acta* **1978**, *537*, 185.

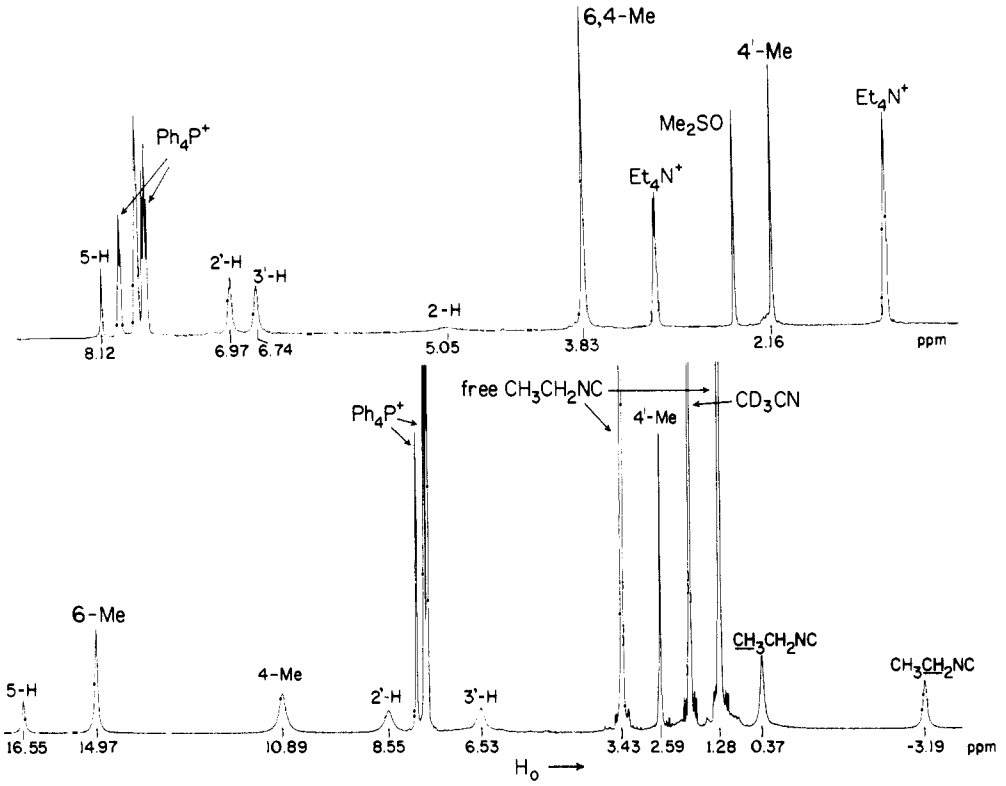

Figure 2. ^{1}H NMR spectra of $[Fe_4S_4(LS_3)(CN)]^{2-}$ (**4**, upper) in Me_2SO solution and $[Fe_4S_4(LS_3)(EtNC)_3]^{1-}$ (**6**, lower) in CD_3CN solution at 297 K; signal assignments are indicated.

flow through the sample region. The powder sample was weighed into a no. 5 gel cap and mixed with a measured amount of mineral oil to form a mull. The gel cap halves were secured together with superglue before being frozen in liquid nitrogen. The control sample consisted of a measured amount of mineral oil in a matching gel cap prepared under the same conditions. Sample and control were each separately suspended near the center of a plastic straw, which was long enough to be undetected during data collection. The nuclear susceptibilities of the protons in the gel cap and mineral oil were of no consequence in these measurements.[16] The Curie law intercept of the difference data (sample minus control) at each field was adjusted to remove the field dependence caused by ferromagnetic impurities in the gel caps. Fitting to the data sets was accomplished by using the nonlinear simplex method of Nelder and Mead[17] to find the spin Hamiltonian parameters yielding the minimum in the standard discrepancy factor χ^2. Magnetization curves were calculated as previously described.[16] The final fit was the best of 10, each started at a randomly selected point in parameter space. Uncertainties in the fit parameters were estimated by Monte Carlo simulations. For these simulations, the added noise was comparable to the noise in the original data.

Results and Discussion

The following clusters **3–11** are of principal interest in this work; of these, **3–9** are of the site-differentiated type **2**.

$[Fe_4S_4(LS_3)Cl]^{2-}$	**3**
$[Fe_4S_4(LS_3)(CN)]^{2-}$	**4**
$[Fe_4S_4(LS_3)(MeNC)_3]^{1-}$	**5**
$[Fe_4S_4(LS_3)(EtNC)_3]^{1-}$	**6**
$[Fe_4S_4(LS_3)(t\text{-}BuNC)_3]^{1-}$	**7**
$[Fe_4S_4(LS_3)(C_6H_{11}NC)_3]^{1-}$	**8**
$[Fe_4S_4(LS_3)(2,6\text{-}Me_2C_6H_3NC)_3]^{1-}$	**9**
$[Fe_4S_4Cl_2(t\text{-}BuNC)_6]$	**10**
$[Fe_4S_4Cl_4]^{2-}$	**11**

Cluster Reactions with Isonitriles. The large majority of anionic ligands thus far tested[2,4-7] bind quantitatively to cluster **3** at the 1 mM concentration level in solvents such as acetonitrile and Me_2SO. Chloride is displaced and the product cluster can be recognized by ^{1}H NMR spectral differences compared to the spectrum of **3**, which has been reported earlier.[2] For example, reaction 1 proceeds to completion with 1 equiv of cyanide, and

$$[Fe_4S_4(LS_3)Cl]^{2-} + CN^- \rightarrow [Fe_4S_4(LS_3)(CN)]^{2-} + Cl^- \quad (1)$$

product cluster **4** exhibits the spectrum in Figure 2. The cluster was not isolated, but was identified by its ^{1}H NMR spectrum. All resonances undergo small shifts compared to those of **3**; e.g., the 5-H signal (Figure 1), which is usually very sensitive to the nature of the ligand at the unique site, changes from 8.23 ppm in **3** to 8.12 ppm in **4**. The chemical shifts of **4** are entirely typical of clusters of type **2** with an $S = 0$ ground state. However, the behavior of isonitriles, strong-field ligands generally comparable to cyanide, is entirely different.

The ^{1}H NMR spectrum of the reaction product of cluster **3** with excess ethyl isonitrile is also shown in Figure 2. The resonances of ring protons and methyl groups of the arms experience pronounced downfield shifts compared to **3**. Even the signals of the legs, which are not directly attached to the core, are displaced relative to their positions in **3**. Integration of bound isonitrile vs LS_3 ligand resonances demonstrates the presence of three isonitriles per cluster. Isonitriles RNC with R = Me, *t*-Bu, C_6H_{11}, and $2,6\text{-}Me_2C_6H_3$ act similarly in terms of 3-fold ligation and large chemical shifts. From these shifts in acetonitrile and Me_2SO and $\mu_{eff} = 5.35\mu_B$ in Me_2SO (297 K) for **7**, the product clusters **5–9** are considerably more paramagnetic than **3**. Titration of cluster **3** with RNC in acetonitrile or Me_2SO solutions demonstrated a simultaneous increase and decrease in the concentrations of $[Fe_4S_4(LS_3)(RNC)_3]^{1-}$ and **3**, respectively. No other species were detected. Consequently, the overall equilibrium reaction 2 proceeds. The spectra of clusters **5–9** generated in this way are consistent with *trigonal* symmetry. So also are the two isonitrile stretching frequencies (2123 and 2153 cm^{-1}) of (Ph_4P)[**7**], isolated from reaction system 2 containing a 10-fold excess of ligand. These results indicate that the three RNC ligands bind at the unique Fe subsite. Although no diffraction-quality crystals of any $[Fe_4S_4(LS_3)(RNC)_3]^{1-}$ compound have been obtained, the structure of a related cluster (vide infra) substantiates the viability

$$[Fe_4S_4(LS_3)Cl]^{2-} + 3RNC \rightleftharpoons [Fe_4S_4(LS_3)(RNC)_3]^{1-} + Cl^- \quad (2)$$

(16) Day, E. P.; Kent, T. A.; Lindahl, P. A.; Münck, E.; Orme-Johnson, W. H.; Roder, H.; Roy, A. *Biophys. J.* **1987**, *52*, 837.
(17) Nelder, J.; Mead, R. *Comput. J.* **1965**, *7*, 308.

Table II. Cluster Binding Equilibria of Isonitriles in Acetonitrile Solutions at 297 K[a,b]

RNC	$K_{eq} \times 10^{-2}$, M^{-2}	ΔG, kcal/mol	ΔH, kcal/mol	ΔS, eu
MeNC	3.8 (0.9)	-3.5 (1)	-23 (1)	-67 (5)
EtNC	14 (4)	-4.3 (2)	c	
t-BuNC	140 (30)	-5.6 (1)	-27 (1)	-74 (3)
$C_6H_{11}NC$	300 (100)	-6.0 (2)	c	
2,6-$Me_2C_6H_3NC$	4900 (600)	-7.7 (1)	c	

[a] Reaction 2. [b] Estimated errors in parentheses. [c] Not determined.

of $Fe(RNC)_3$ coordination. Equilibrium constants for reaction 2 are set out in Table II. These and the thermodynamic features of the reactions are more meaningfully considered after examination of the ground-state electronic structure of the clusters.

Ground-State Electronic Properties. Given the nearly identical isotropically shifted ^1H NMR spectra of clusters **5–9**, it is highly probable that all have a common electronic ground state. Our initial Mössbauer spectroscopic study[9] of the isolated compound (Ph_4P)[**7**] served to show that the unique cluster subsite is low-spin Fe(II). The remaining three Fe atoms give spectra that are remarkably similar to those observed for the protein-bound $[Fe_3S_4]^0$ clusters of *Desulfovibrio gigas* ferredoxin II[18,19] (*Dg* Fd II) and aconitase.[20] Consequently, cluster **7** contains a *spin-isolated* $[Fe_3S_4]^0$ *fragment*, formally composed of 2Fe(III) + Fe(II). The native clusters have been shown by crystallography to have the "voided cubane" structure **12**,[21,22] corresponding to

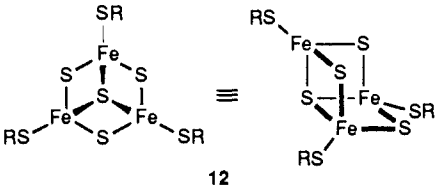

12

the removal of an Fe atom from the Fe_4S_4 structure. Here we provide the results of an investigation of the magnetism of **7** and a more detailed analysis of its Mössbauer spectra. Mössbauer parameters of this cluster are presented in Table III and compared with those of the protein clusters in the same oxidation level. At present, **7** and related clusters are the only non-protein examples of the stabilization of the Fe_3S_4 fragment with the characteristic electronic properties described below.

(a) Native $[Fe_3S_4]^0$ Clusters. Before proceeding further, it is useful to summarize briefly the results obtained for protein-bound $[Fe_3S_4]^0$ clusters, the most intensively studied of which is that in *Dg* Fd II.[18,19] The majority quadrupole doublet of the two observed in a 2:1 ratio in the zero-field Mössbauer spectrum at 4.2 K has parameters indicative of the $Fe^{2.5+}$ oxidation state. The two Fe atoms contributing to this doublet equally share the electron added to the cluster upon reduction of the $[Fe_3S_4]^{1+}$ oxidation level. They are referred to as the delocalized pair (subsites 1 and 2 in Table III). The minority doublet represents high-spin Fe(III) (subsite 3). The spins of the three Fe atoms are coupled to yield a cluster ground state with $S = 2$, which was initially proposed from MCD results[23] and recently demonstrated from magnetization properties.[24] The electronic features of the $S = 2$ manifold can be described by the spin Hamiltonian 3, where D and E are the axial

$$H_e = D(S_z^2 - 2) + E(S_x^2 - S_y^2) + \beta \mathbf{S}\cdot\mathbf{g}\cdot\mathbf{H} \qquad (3)$$

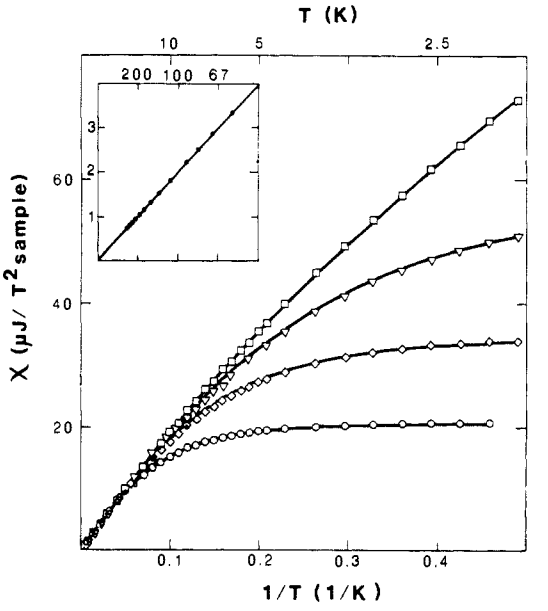

Figure 3. Plots of the magnetic susceptibility vs inverse temperature for amorphous $(Ph_4P)[Fe_4S_4(LS_3)(t\text{-BuNC})_3]$ ((Ph_4P)[**7**]) in mineral oil at the fields 0.20 (□), 1.375 (▽), 2.75 (◇), and 5.50 (○) T over the range 2–270 K. The solid lines were calculated from the $S = 2$ spin Hamiltonian 3 with $D = -2.8$ cm^{-1}, $E/D = 0.31$, and $g_{av} = 2.14$. The amount of paramagnetic ($S = 2$) cluster was treated as a fitting parameter; in these experiments the sample contained 5.8 μmol of paramagnetic cluster. The same sample was used in the Mössbauer experiments in Figures 4 and 5; no paramagnetic impurity was detectable by Mössbauer spectroscopy. The inset shows the same data in detail above 50 K and illustrates Curie behavior; the solid circles represent overlapping data at all four fields at each temperature.

and rhombic zero-field-splitting (ZFS) parameters, respectively, and $\mathbf{g}$ is the $\mathbf{g}$ tensor of the multiplet; g_x, g_y, and g_z are expected to be slightly larger than 2. With E/D fixed at 0.23, the magnetization data of *Dg* Fd II could be fitted well with $D = -2.7$ cm^{-1}.[24]

For the analysis of Mössbauer spectra recorded in strong applied fields, eq 3 needs to be augmented by terms describing the magnetic hyperfine interactions with the ^{57}Fe nuclei. In eq 4, the index i sums over the three sites. For *Dg* Fd II and cluster **7**, we have found that the electric field gradient (EFG) tensors [principal components, V_{xx}, V_{yy}, V_{zz}; $\eta = (V_{xx} - V_{yy})/V_{zz}$] are rotated relative to the ZFS tensor.

$$H_{hf} = \sum_{i=1}^{3} [\mathbf{S}\cdot\mathbf{A}(i)\cdot\mathbf{I}(i) - \mathbf{g}_n\beta_n\mathbf{H}\cdot\mathbf{I}(i) + H_Q(i)] \qquad (4)$$

$$H_Q = [eQV_{zz}/12][3I_z^2 - 15/4 + \eta(I_x^2 - I_y^2)] \qquad (5)$$

Evaluation of the *Dg* Fd II spectra by means of $H = H_e + H_{hf}$ and subsequent analysis of the magnetic hyperfine coupling tensors $\mathbf{A}(i)$ with a spin-coupling model lead to the following insight into the coupling mechanism.[18,19] The three Fe atoms of the cluster are coupled by the antiferromagnetic exchange $J\mathbf{S}_i\cdot\mathbf{S}_j$. Additionally, the Fe atoms of the delocalized pair interact by double exchange.[19] Experimentally, it has been found that the pair has dimer spin $S_{12} = {}^9/_2$. The local spin of the Fe^{III} site, $S_3 = {}^5/_2$, is aligned antiparallel to S_{12} to produce the $S = 2$ system spin. Papaefthymiou et al.[19] have considered that the $S_{12} = {}^9/_2$ pair spin arises from strong double exchange (B), i.e., $|B/J| > 2$. However, a similar ground state can result from weak spin coupling as well.[25]

(b) Magnetization. Shown in Figure 3 are the magnetization data of cluster **7** collected at four field strengths ranging from 0.20 to 5.50 T over the temperature range 2–270 K. We have fitted the data to the $S = 2$ spin Hamiltonian of eq 3 with the

(18) Moura, J. J. G.; Moura, I.; Kent, T. A.; Lipscomb, J. D.; Huynh, B. H.; LeGall, J.; Xavier, A. V.; Münck, E. *J. Biol. Chem.* **1982**, *257*, 6259.
(19) Papaefthymiou, V.; Girerd, J.-J.; Moura, I.; Moura, J. J. G.; Münck, E. *J. Am. Chem. Soc.* **1987**, *109*, 4703.
(20) Surerus, K. K.; Kennedy, M. C.; Beinert, H.; Münck, E. *Proc. Natl. Acad. Sci. U.S.A.* **1989**, *86*, 9846.
(21) Kissinger, C. R.; Adman, E. T.; Sieker, L. C.; Jensen, L. H. *J. Am. Chem. Soc.* **1988**, *110*, 8721.
(22) Robbins, A. H.; Stout, C. D. *Proc. Natl. Acad. Sci. U.S.A.* **1989**, *86*, 3639; *Proteins* **1989**, *5*, 289.
(23) Thomson, A. J.; Robinson, A. E.; Johnson, M. K.; Moura, J. J. G.; Moura, I.; Xavier, A. V.; LeGall, J. *Biochim. Biophys. Acta* **1981**, *670*, 93.
(24) Day, E. P.; Peterson, J.; Bonvoisin, J. J.; Moura, I.; Moura, J. J. G. *J. Biol. Chem.* **1988**, *263*, 3684.

(25) We thank Dr. I. Bertini for bringing the weak double exchange solution to our attention.

Table III. Mössbauer Parameters of Clusters **7** and **10** and Comparison with *Desulfovibrio gigas* Fd II and Beef Heart Aconitase (4.2 K)

cluster	subsite	mm/s		MHz			
		δ[b]	ΔE_Q	A_x	A_y	A_z	β,[c] deg
7[a]	1	0.46	+1.21	−18.5 (2)	−15 (5)	−15 (1)	20
	2	0.47	+1.49	−18.5 (2)	−15 (5)	−15 (1)	30
	3	0.34	−0.59	+11 (2)	+15 (5)	+17 (1)	0
	4[d]	0.20	0.50[e]				
Dg Fd II[f]	1, 2	0.46	+1.47	−20.5	−20.5	−16.4	20
	3	0.32	−0.52	+13.7	+15.8	+17.3	16
aconitase[g]	1	0.46	+1.15	−19	−19	−16	25
	2	0.49	+1.46	−19	−19	−15	15
	3	0.31	+0.56	+17	+17	+16.5	50
10	1	0.41	0.60				
	2[d]	0.19	0.45				

[a] The spectra of **7** were fitted with an $S = 2$ spin Hamiltonian (eqs 3 and 4) for $D = -2.8$ cm^{-1} and $E/D = 0.33$. Numbers in parentheses are the estimated uncertainties in the A value for the least significant digit. The EFG asymmetry parameter $\eta = 0$ for sites 1 and 2 and $\eta = +2.5$ for site 3. All simulations were performed in the slow fluctuation limit and a line width of 0.33 mm/s was used. [b] Relative to Fe metal at room temperature. [c] Angle between the z axes of EFG and zero-field-splitting tensors. [d] Low-spin Fe(II). [e] Sign of ΔE_Q and η value could not be determined; for the simulations, $\Delta E_Q > 0$ and $\eta = 0$. [f] Reference 18. [g] Reference 20.

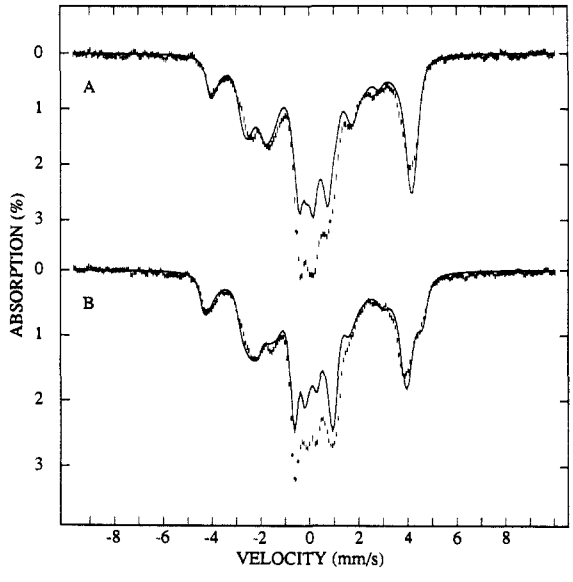

Figure 4. Mössbauer spectra of $(Ph_4P)[Fe_4S_4(LS_3)(t\text{-BuNC})_3]$ ((Ph_4P)[**7**]) as an amorphous solid at 4.2 K in fields of 2.5 (A) and 4.0 (B) T applied parallel to the γ-radiation. The solid lines are spectral simulations using the parameters in Table III. For reasons given in the text, the theoretical spectra are plotted to represent 85% of the absorption area.

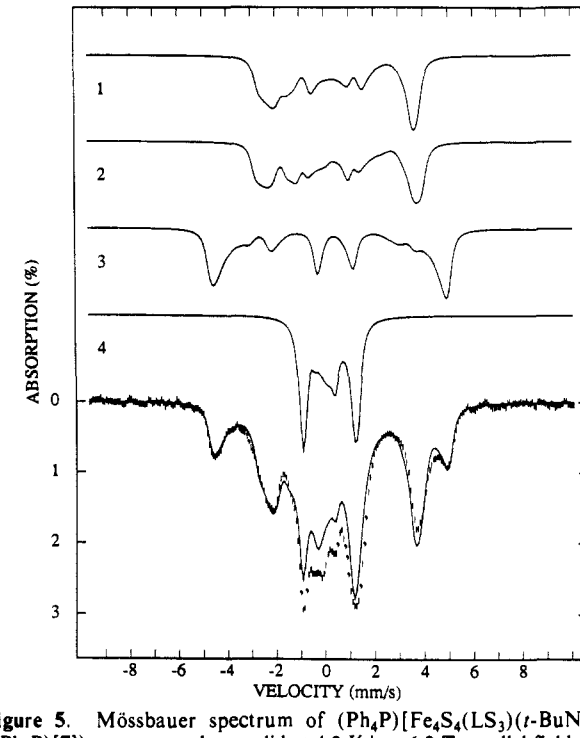

Figure 5. Mössbauer spectrum of $(Ph_4P)[Fe_4S_4(LS_3)(t\text{-BuNC})_3]$ ((Ph_4P)[**7**]) as an amorphous solid at 4.2 K in a 6.0-T parallel field. The solid lines are theoretical curves generated with the parameter set of Table III for subsites 1–4. For reasons given in the text, the sum spectrum is plotted to represent 90% of the absorption. The observation that the magnetic splitting of the spectrum of the Fe^{3+} subsite 3 increases with increasing applied field implies $A_3 > 0$. Subsites 1 and 2 ($Fe^{2.5+}$) have $A_{1,2} < 0$ and the low-spin Fe^{2+} subsite 4 is diamagnetic.

assumption that $g_x = g_y = g_z = g_{av}$. From these fits we obtain $D = -2.8 \pm 0.1$ cm^{-1}, $E/D = 0.31 \pm 0.02$, and $g_{av} = 2.14 \pm 0.02$. These parameters agree well with those of *Dg* Fd II.[24] We stress that the data cannot be fit properly unless $S = 2$. The high-temperature susceptibility data, shown in the inset of Figure 3, indicate no deviation from $S = 2$ Curie law behavior up to 270 K. The solution magnetic moment of $5.35\mu_B$ is in accordance with a spin-quintet ground state.

(c) Mössbauer Spectra. The zero-field spectrum of **7** has been given earlier.[9] Spectra of this cluster recorded in parallel applied fields of 2.5, 4.0, and 6.0 T are set out in Figures 4 and 5. We have performed computer simulations using the $S = 2$ Hamiltonian $H = H_e + H_{hf}$ and the methodology of spectral analysis discussed elsewhere.[18-20] Because these spectra are quite similar to those analyzed for *Dg* Fd II[18,19] and aconitase,[20] we used the parameters of the protein clusters as a starting set. The results of the spectral simulations are presented in Figures 4 and 5; the latter shows a decomposition of the 6.0-T spectrum into the spectra of the four subsites. The parameter set used is listed, together with those of *Dg* Fd II and aconitase, in Table III. The theoretical spectra in Figures 4 and 5 are plotted to represent 90 and 85% of the spectral areas, respectively, for two reasons. First, ^{1}H NMR spectra of (Ph_4P)[**7**] in CD_3CN indicated that ~5% of the iron of the Mössbauer sample was in the form of an $S = 0$ $[Fe_4S_4]^{2+}$ cluster; such a species will contribute to the central parts of the spectra. Second, consideration of the entire set of spectra suggested that the electronic spins of a fraction of molecules in the sample, perhaps 5% at 6.0 T and 10% at 2.5 T, do not relax slowly on the time scale of Mössbauer spectroscopy. Intermediate or fast relaxation would result in the transfer of absorption toward the centers of the spectra.[26]

Our claim that the unique cluster subsite of **7**, containing the $Fe(t\text{-BuNC})_3$ group, is diamagnetic[9] was based on the observation that the magnetic splitting of subsite 4 (Table III) can be at-

(26) Most likely, the faster relaxing spins belong to molecules in the powder sample that are oriented such that the y axis of the ZFS tensor is along the applied field; for this orientation and for the ZFS parameters quoted, the two lowest electronic levels remain close, to within 1.0 cm^{-1} even at 6.0 T. Initially, we were misled by the relaxation phenomenon, and we fitted the data with $D = -7$ cm^{-1}. This unusual result prompted the magnetization study. After recognizing the relaxation problem, we were able to fit the outer absorption features using $D = -3$ cm^{-1} and $E/D = 0.33$. When the susceptibility data became available, we adjusted D to -2.8 cm^{-1}.

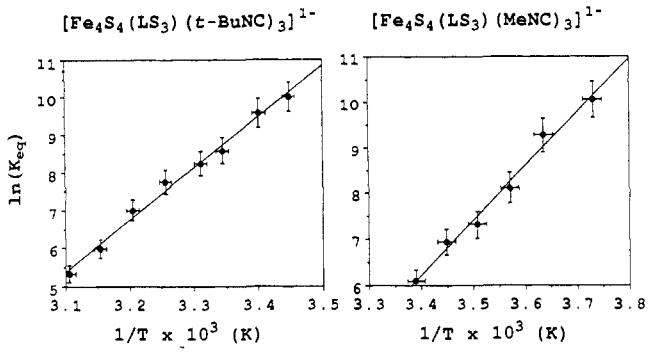

Figure 6. Temperature dependencies of the equilibrium constants of reaction 2 for the formation of $[Fe_4S_4(LS_3)(RNC)_3]^{1-}$ [R = Me (**5**), *t*-Bu (**7**)] in acetonitrile solutions.

tributed solely to the action of the applied field through the nuclear Zeeman term. As can be seen from an inspection of Figure 5, the sharp absorption feature at zero Doppler velocity corresponds to the low-energy line of the subsite 4 spectrum. By fitting subsite 4 to this feature, an upper limit for the possible magnetic hyperfine interactions $A_4\mathbf{S}\cdot\mathbf{I}_4$ can be set. From spectral simulations, we conclude that $|A_4| < 0.2$ MHz, which is less than 1.5% of the A values observed for the other three subsites and is consistent with diamagnetism ($A_4 = 0$).[27]

The Mössbauer spectrum of cluster **7** at 4.2 K exhibits four distinct doublets. In our initial account,[9] we reported that the 270 K spectrum can be fitted with two doublets in a 3:1 area ratio. This observation led us to suggest that the $[Fe_3S_4]^0$ fragment exhibits the property of valence-detrapping above 100 K. However, further studies have revealed that the quadrupole splittings of the delocalized pair have a pronounced temperature dependence. Thus, at 270 K the splittings of subsites 1 and 2 have decreased ($\Delta E_{Q1} = 0.66$ mm/s and $\Delta E_{Q2} = 0.79$ mm/s) and the doublets of subsites 1–3 have merged into one feature.[28] In contrast, for the protein-bound clusters, the splittings of subsites 1 and 2 depend only weakly on temperature. Most likely, this behavior reflects different spatial orientations of the terminal thiolate ligands in the proteins and in **7**. This is suggested by the finding that $(Bu_4N)_2[Fe_4S_4(SPh)_4]$ exhibits strongly temperature dependent ΔE_Q values, while the splittings of $(Et_4N)_2[Fe_4S_4(SCH_2Ph)_4]$ vary only very little with temperature.[29]

The Mössbauer and magnetic susceptibility results demonstrate beyond doubt that *the electronic properties of the Fe_3S_4 fragment of cluster 7 are remarkably similar to those of $[Fe_3S_4]^0$ cores of proteins*. Both the synthetic and native clusters have an $S = 2$ ground state with virtually identical zero-field splittings. Table III shows that the hyperfine parameters of *Dg* Fd II, aconitase, and **7** are essentially the same. Because this remarkable similarity holds for the hyperfine tensors, it follows that the two cluster types have the same spin-coupling mechanism; viz., $S_{12} = {}^9/_2$ of the delocalized pair and $S_3 = {}^5/_2$ of the Fe^{3+} site are aligned antiparallel to afford the $S = 2$ state. A different value of S_{12} would express itself by drastically different A tensors.[19] Given the common spin ground state, the impressive similarity among parameter sets, and the different structural environments, we consider it highly probable that the spin-coupled $S = 2$ ground state of $[Fe_3S_4]^0$ is an intrinsic property of this cluster; i.e., it is not conditioned by elements of protein structure and environment.

Cluster Binding Equilibria and Thermodynamics. Equilibrium constants for reaction 2 were determined by monitoring the concentrations of free RNC, initial cluster **3**, and product clusters **5–9** by means of integrated NMR signal intensities. Thermodynamic parameters for the formation of **5** and **7** were obtained from spectra recorded in the ca. 270–300 K range.[30] The equilibrium and thermodynamic data are collected in Table II. Plots of the temperature dependencies of the equilibrium constants of the clusters are available in Figure 6. When the isonitrile clusters are fully formed, the solutions assume a purplish-brown color. Attempts to bind additional cyanide to cluster **4** by use of 2–4 equiv of the ligand afforded ^{1}H NMR spectra suggestive of displacement of the coordinating arms. In comparison, anaerobic solutions of **5–9** with excess isonitrile appear to be indefinitely stable.

Equilibrium constants of reactions with alkyl isonitriles follow the gas-phase proton affinity sequence 6 (kcal/mol) determined

$$\text{MeNC (199.3)} < \text{EtNC (203.7)} < t\text{-BuNC (207.5)} \quad (6)$$

by ion cyclotron resonance.[31] The more basic the isonitrile by this measure, the stronger the binding. Proton affinities of arene isonitriles have not been reported. Steric effects appear to be inconsequential in setting the stability order of the isonitrile clusters.

The reactions 2 provide interesting cases of $|\Delta H| > |T\Delta S|$, with the latter term ~85% of ΔH. These reactions are spontaneous because of the enthalpy changes. The large entropy changes are consistent with the net consumption of two molecules. The failure to detect clusters with one or two bound isonitriles becomes understandable upon the determination that the unique Fe subsite is low-spin when three ligands are bound. In the case of reaction 7 with L = bipy or phen, the orders of overall formation constants[32]

$$[Fe(OH_2)_6]^{2+} + 3L \rightleftharpoons [FeL_3]^{2+} + 6H_2O \quad (7)$$

and heats of complexation[33-35] (absolute values) are $\beta_3 > \beta_2 > \beta_1$ and $\Delta H_3 > \Delta H_2 > \Delta H_1$. However, the *stepwise* formation constants and enthalpies behave as $K_{0-1} > K_{1-2} \ll K_{2-3}$[36] and $\Delta H_{0-1} \approx \Delta H_{1-2} < \Delta H_{2-3}$, with the difference in the last two values being about 9–13 kcal/mol depending on the data chosen. Binding of the third ligand is more favorable than for the first two because the other two complexes are paramagnetic whereas $[FeL_3]^{2+}$ is diamagnetic. Consequently, conversion from $[FeL_2(OH_2)_2]^{2+}$ to $[FeL_3]^{2+}$ results in a gain in ligand field stabilization energy of $-2(\Delta_{0.3} - \Delta_{0.2})$. Reaction 7 with L = en shows no such effects;[37] in this series all complexes are high-spin, and there is no special d-electron stabilization of $[Fe(en)_3]^{2+}$. We interpret reaction 2 to be analogous to reaction 7, in which event only $[Fe_4S_4(LS_3)(RNC)_3]^{1-}$, with its local diamagnetic site $Fe^{II}S_3(RNC)_3$, accumulates to a measurable extent.

Preparation of $[Fe_4S_4Cl_2(t\text{-BuNC})_6]$. In the absence of any crystals of $[Fe_4S_4(LS_3)(RNC)_3]^{1-}$ compounds suitable for x-ray studies, related clusters that might contain a $Fe(RNC)_3$ subsite

(27) We comment briefly on the uncertainties of the A values in Table III. The spectra of Figures 4 and 5 are dominated by the properties of the lowest level of the spin quintet. For $D < 0$ and $E/D = 0.33$, this level has an easy axis of magnetization along the z axis and the Mössbauer spectra are, therefore, quite sensitive to $A_z(i)$. For applied fields above 4.0 T, increased level mixing leads to an increased sensitivity of the spectra to $A_x(i)$. Through the whole range of applied fields, the spectra are quite insensitive to $A_y(i)$. Table III indicates that the z axes of the EFG tensors of subsites 1 and 2 are tilted relative to the z axis of the ZFS tensor. While it is not surprising that these tensors are not aligned, the angle β is strongly correlated with values of ΔE_Q, η, and A_z; the quoted values of β are, therefore, quite soft. On the other hand, as shown in Table III, β-values of 15–30° were obtained from protein-bound Fe_3S_4 clusters as well.

(28) Cf.: Figure 1 of ref 9.

(29) Frankel, R. B.; Averill, B. A.; Holm, R. H. *J. Phys. (Paris)* **1974**, *35*, C6.

(30) This narrow range was necessitated in order to prevent reaction 2 from shifting nearly completely in one direction or the other, in which event equilibrium constants could not be determined accurately.

(31) Meot-Ner, M.; Karpas, Z.; Deakyne, C. A. *J. Am. Chem. Soc.* **1986**, *108*, 3913.

(32) Irving, H.; Mellor, D. H. *J. Chem. Soc.* **1962**, 5222. bipy = 2,2′-bipyridyl, phen = 1,10-phenanthroline.

(33) Baxendale, J. H.; George, P. *Trans. Faraday Soc.* **1950**, *46*, 55.

(34) Davies, K. L.; Dunning, K. W. *J. Chem. Soc.* **1965**, 4168.

(35) Lahiri, S. C.; Aditya, S. *Z. Phys. Chem. N. F.* **1964**, *41*, 173.

(36) There is, however, some question as to the accuracy of K_{1-2} values: Brisbin, D. A.; McBryde, W. A. E. *Can. J. Chem.* **1963**, *41*, 1135. McBryde, W. A. E. *A Critical Review of Equilibrium Data for Proton and Metal Complexes of 1,10-Phenanthroline, 2,2′-Bipyridyl and Related Compounds*; IUPAC Chemical Data Series 17; Pergamon Press: New York, 1978; pp 7–13.

(37) Ciampolini, M.; Paoletti, P.; Sacconi, L. *J. Chem. Soc.* **1960**, 4553. en = ethylenediamine.

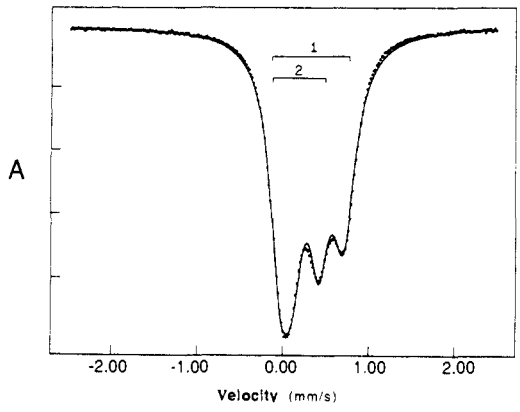

Figure 7. Mössbauer spectrum of polycrystalline $[Fe_4S_4Cl_2(t\text{-BuNC})_6]$ (**10**) in zero applied magnetic field at 4.2 K. The solid line is a fit of the spectrum using the parameters of Table III; locations of the quadrupole doublets of the two subsites are indicated.

were sought by other preparative routes. After some experimentation, reaction 8, conducted with 20 equiv of isonitrile under

$$[Fe_4S_4Cl_4]^{2-} + 6t\text{-BuNC} \xrightarrow{\text{THF}} [Fe_4S_4Cl_2(t\text{-BuNC})_6] + 2Cl^- \quad (8)$$

reflux, afforded the dark purple cluster **10** in 60% yield from the Ph_4P^+ salt of precursor chloro cluster **11**. The reaction is assisted by the insolubility of Ph_4PCl in THF, a solvent that favors the formation of a neutral product. Under these conditions, we have not detected a less substituted product; among other observations, the initial cluster and 10 equiv of *t*-BuNC under reflux gave no reaction after 1 h.

Cluster **10** in dichloromethane solution exhibits two *t*-Bu resonances in a 2:1 ratio, consistent with the C_2 symmetry observed in the solid state (vide infra). Consequently, the cluster does not disproportionate in this solvent. In contrast, the anionic clusters $[Fe_4S_4L_4]^{2-}$ with mixed terminal ligands rapidly equilibrate to statistical mixtures of other charged clusters in solvents such as acetonitrile and Me_2SO.[4] This behavior has necessitated the synthesis of ligand **1** in order to achieve a 3:1 subsite differentiation. However, in a low-dielectric solvent where disproportionation of a neutral molecule would afford charged products, this process is likely to be slow or absent, as is the case with **10**.[38]

The Mössbauer spectrum of cluster **10**, shown in Figure 7, consists of two partially resolved quadrupole doublets. It can be satisfactorily fit with two doublets of 1:1 intensity ratio and the parameters of Table III. Doublet 2 has the smaller isomer shift and quadrupole splitting, the values of which are consistent with low-spin Fe(II). The close agreement of the parameters of subsite 4 in **7** and subsite 2 in **10** ensures that the Fe atoms in these subsites are essentially identical. It follows that in cluster **10** there is a *spin-isolated* $Fe^{III}_2S_2$ *fragment*. The magnetic moment $\mu_{Fe} = 1.41\mu_B$ (CD_2Cl_2, 297 K) is the same as those of the antiferromagnetically coupled complexes $[Fe_2S_2L_4]^{2-}$ (L = Cl^-, RS^-) at ambient temperature ($1.39-1.42\mu_B$[10,39]).

Structure of $[Fe_4S_4Cl_2(t\text{-BuNC})_6]$. The structure of cluster **10** is shown in Figure 8. It has the familiar cubane-type stereochemistry with an imposed 2-fold axis passing through faces Fe(1,1')S(2,2') and Fe(2,2')S(1,1'). All Fe_2S_2 faces are nonplanar rhombs. Selected bond distances and angles are collected in Table IV. It is immediately evident that the cluster contains two symmetry-related $Fe(t\text{-BuNC})_3$ subsites in distorted octahedral coordination and two conventional tetrahedral subsites with terminal chloride ligands.

(a) The Core. With six short (2.248 Å) and six long (2.360 Å) Fe–S bonds, the $[Fe_4S_4]^{2+}$ core markedly departs from the usual structure of four short and eight long bonds in $[Fe_4S_4L_4]^{2-}$ clusters.[40-43] The unprecedented core geometry is manifested in several other ways. The core face Fe(2,2')S(1,1') has an Fe–Fe distance of 2.741 (3) Å and other dimensions quite similar to those of a rhombic face of $[Fe_4S_4Cl_4]^{2-}$.[40] However, the opposite face, Fe(1,1')S(2,2'), at whose subsites the isonitriles are bound, has longer Fe–S and Fe–Fe separations. The latter distance, 3.444 (3) Å, is 0.70 Å longer than that in the opposite face. These faces are connected by the shortest and longest Fe–S bonds, parallel to the 2-fold axis with two at 2.251 (2) Å and two at 2.375 (3) Å. The atoms comprising these faces are decidedly noncoplanar, the deviations from unweighted least-squares planes being ±0.100 Å for Fe(1,1')S(2,2') and ±0.167 Å for Fe(2,2')S(1,1'). In the remaining four faces, the Fe–Fe distances are intermediate [2.994

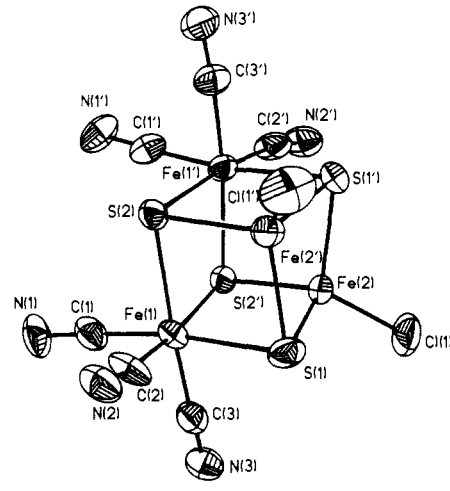

Figure 8. Structure of $[Fe_4S_4Cl_2(t\text{-BuNC})_6]$ (**10**) showing the atom labeling scheme and 30% probability ellipsoids but omitting the *tert*-butyl groups; primed and unprimed atoms are related by the 2-fold axis.

Table IV. Selected Distances and Angles for $[Fe_4S_4Cl_2(t\text{-BuNC})_6]$

	Distances, Å		
Fe(1)–Fe(1')	3.444 (3)	Fe(1)–S(1)	2.375 (3)
Fe(1)–Fe(2)	2.994 (3)	Fe(1)–S(2)	2.353 (2)
Fe(2)–Fe(2')	2.741 (3)	Fe(1)–S(2')	2.353 (2)
		mean	2.360
Fe(1)–C(1)	1.774 (11)		
Fe(1)–C(2)	1.825 (11)		
Fe(1)–C(3)	1.868 (11)	Fe(2)–S(1)	2.243 (3)
mean	1.822	Fe(2)–S(2')	2.251 (2)
		Fe(2)–S(1')	2.250 (3)
Fe(2)–Cl(1)	2.214 (4)	mean	2.248
	Angles, deg		
S(1)–Fe(1)–C(1)	171.9 (4)	S(1)–Fe(1)–S(2)	95.2 (1)
S(1)–Fe(1)–C(2)	84.2 (4)	S(2)–Fe(1)–S(2')	85.1 (1)
S(1)–Fe(1)–C(3)	87.5 (3)	S(1)–Fe(1)–S(2')	95.5 (1)
S(2)–Fe(1)–C(1)	91.0 (3)	S(1)–Fe(2)–S(1')	102.2 (1)
S(2)–Fe(1)–C(2)	87.0 (3)	S(1)–Fe(2)–S(2')	102.3 (1)
S(2)–Fe(1)–C(3)	170.7 (4)	S(2')–Fe(2)–S(1')	101.7 (1)
C(1)–Fe(1)–C(2)	90.9 (5)	Fe(1)–S(1)–Fe(2)	80.8 (1)
C(1)–Fe(1)–C(3)	87.3 (4)	Fe(1)–S(1)–Fe(2')	81.1 (1)
C(2)–Fe(1)–C(3)	102.1 (5)	Fe(2)–S(1)–Fe(2')	75.2 (1)
C(1)–Fe(1)–S(2')	90.2 (4)	Fe(1)–S(2)–Fe(1')	94.1 (1)
C(2)–Fe(1)–S(2')	172.1 (3)	Fe(1)–S(2)–Fe(2')	81.6 (1)
C(3)–Fe(1)–S(2')	85.8 (4)	Fe(1')–S(2)–Fe(2')	81.1 (1)
Fe(1)–C(1)–N(1)	177.3 (8)	Cl(1)–Fe(2)–S(1)	115.5 (1)
Fe(1)–C(2)–N(2)	171.8 (10)	Cl(1)–Fe(2)–S(1')	117.2 (1)
Fe(1)–C(3)–N(3)	173.7 (10)	Cl(1)–Fe(2)–S(2')	115.7 (1)

(38) An apparently similar cluster, $[Fe_4S_4I_2(SPPh_3)_2]$, has been prepared and its structure determined: Saak, W.; Pohl, S. *Z. Naturforsch.* **1988**, *43B*, 813.

(39) Gillum, W. O.; Frankel, R. B.; Foner, S.; Holm, R. H. *Inorg. Chem.* **1976**, *15*, 1095.

(40) Bobrik, M. A.; Hodgson, K. O.; Holm, R. H. *Inorg. Chem.* **1977**, *16*, 1851.

(41) Berg, J. M.; Holm, R. H. In *Metal Ions in Biology*; Spiro, T. G., Ed.; Interscience: New York, 1982; Vol. 4, Chapter 1.

(42) Carney, M. J.; Papaefthymiou, G. C.; Spartalian, K.; Frankel, R. B.; Holm, R. H. *J. Am. Chem. Soc.* **1988**, *110*, 6084, and references therein.

(43) Que, L., Jr.; Bobrik, M. A.; Ibers, J. A.; Holm, R. H. *J. Am. Chem. Soc.* **1974**, *96*, 4168.

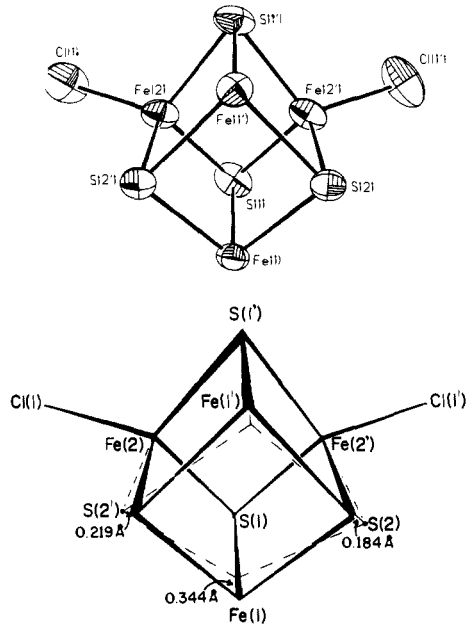

Figure 9. Top: view of the $Fe_4S_4Cl_2$ portion of $[Fe_4S_4Cl_2(t\text{-BuNC})_6]$ (**10**). Bottom: a comparison of the core sizes of **10** (—) and $[Fe_4S_4Cl_4]^{2-}$[39] (---). One $Fe_2S_2Cl_2$ fragment of $[Fe_4S_4Cl_4]^{2-}$ was fit to the (Fe(2,2')S(1,1')Cl(1,1')) portion of **10** by using a molecular fitting routine. The root-mean-square deviation of the positions of the six atoms ($Fe_2S_2Cl_2$) from the two structures is 0.047 Å.

Table V. $[Fe_4S_4]^z$ Core Volumes of Clusters

cluster	z	V, Å^3 Fe_4	S_4	Fe_4S_4	ref
$[Fe_4S_4Cl_4]^{2-}$	2+	2.49	5.43	9.70	39
$[Fe_4S_4Cl_2(t\text{-BuNC})_6]$	2+	3.21	4.78	11.04	*a*
$[Fe_4S_4(SPh)_4]^{2-}$	2+	2.41	5.54	9.55	42
$[Fe_4S_4(SPh)_4]^{3-}$	1+	2.43[b]	5.76	9.73	43
	1+	2.53[c]	5.75	10.00	44
$[Fe_4S_4(CO)_{12}]$	0	4.85	3.53	13.10	45

[a] This work. [b] Me_4N^+ salt. [c] Me_4N^+ salt, 2MeCN solvate.

(3) Å] and the atoms are more nearly coplanar (Fe, 0.041 to 0.055 Å; S, −0.043 to −0.052 Å).

The unusual core geometry of **10** can be appreciated by the comparison with structurally typical cluster **11**[40] in Figure 9. The $Fe_2S_2Cl_2$ fragment of **10** has been fit to the most nearly congruent fragment of **11**, resulting in a rms deviation of 0.047 Å in atom positions. The distances given convey the deviation from congruency of the remaining Fe and S atoms of **10** and **11**. These values are substantial and further reveal that the core of **10** is the larger. We have previously introduced volumes, calculated from atom coordinates, as a convenient means of comparing differences in core sizes.[40] A set of core volumes[41,43-45] is collected in Table V. Indeed, the core of **10** is 13.8% larger than that of **11**. Core volumes are considered further below.

(b) The Tetrahedral Fe(III) Subsite. The Fe(2,2')S(1,1') fragment of **10** may be likened to the $[Fe_2S_2]^{2+}$ core of $[Fe_2S_2Cl_4]^{2-}$[40] and other binuclear $[Fe_2S_2L_4]^{2-}$ species,[41] all of which contain antiferromagnetically coupled, high-spin Fe(III). The magnetic moment of the cluster, given above, is consistent with this situation. The dimensions of the fragment are somewhat larger than those of the binuclear core, as shown by the Fe–Fe distance of 2.741 (3) Å compared to 2.716 (1) Å. The terminal Fe–Cl distance [2.214 (4) Å] is shorter than that of the dimer (mean 2.252 Å) and is indistinguishable from the mean value of

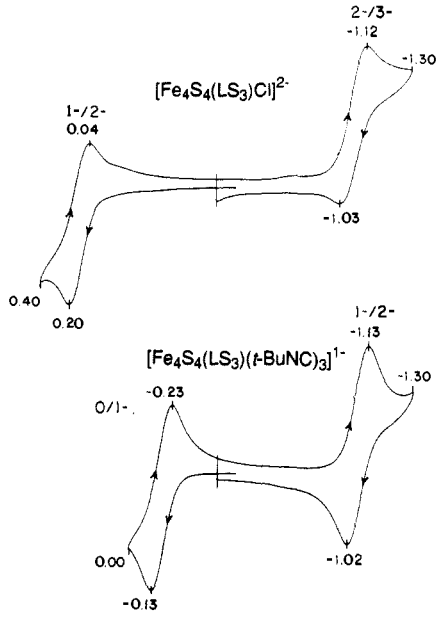

Figure 10. Cyclic voltammograms of $[Fe_4S_4(LS_3)Cl]^{2-}$ (**3**) and $[Fe_4S_4(LS_3)(t\text{-BuNC})_3]^{1-}$ (**7**) in dichloromethane solutions at 50 mV/s and 297 K; peak potentials vs SCE are indicated.

11 [2.216 (2) Å], which is a more reduced cluster. It is generally the case that face dimensions of $[Fe_4S_4L_4]^{2-}$ are larger than core dimensions of $[Fe_2S_2L_4]^{2-}$ clusters. Consequently, the structural features of the tetrahedral Fe sites are not inconsistent with Fe(III), although a shorter Fe–Cl distance than that observed might have been expected.

(c) The Diamagnetic Fe(II) Subsite. The two $FeS_3(t\text{-BuNC})_3$ subsites necessarily have *fac* stereochemistry and provide one of the few cases of a trigonal $Fe(RNC)_3$ group.[47] The mean Fe–C bond distance of 1.822 Å is below the range of distances (1.86–1.93 Å[48]) in Fe(II) compounds when such bonds are trans to each other. Data bearing on the effects of other trans ligands are sparse, but distances of 1.72–1.81 Å have been observed.[48a,49] The subsites are well separated from each other by an Fe–Fe distance of 3.444 (3) Å and are closer to the tetrahedral subsites [Fe–Fe, 2.994 (3) Å] than they are to each other. These separations, coupled with the low-spin nature of the subsites, result in effective electronic isolation of them and of the Fe_2S_2 portion containing the tetrahedral subsites. In $[Fe_4S_4L_4]^{2-}$ clusters, Fe–Fe distances are always ca. 2.7 Å and core volumes are usually in the 9.5–9.8-Å^3 range. Reduction of the core to $[Fe_4S_4]^{1+}$ increases the mean Fe–Fe distance slightly and causes a small increase in volume, as shown by the 1.9 and 4.7% changes with $[Fe_4S_4(SPh)_4]^{2-,3-}$ (Table V). A similar increase might have been expected upon reduction to the all-ferrous core $[Fe_4S_4]^0$. However, in the only proven example of a cluster with this core, $[Fe_4S_4(CO)_{12}]$,[46] the Fe–Fe distance is 3.47 Å and the core volume is 13.10 Å^3. The volume of the Fe_4 tetrahedron is larger than that of the S_4 tetrahedron. This is opposite of the case with $[Fe_4S_4L_4]^{2-,3-}$ clusters. Consequently, the carbonyl cluster provides the extreme case of subsite isolation, in which four six-coordinate low-spin Fe(II) atoms actually are positioned outside their S_4 tetrahedron at the longest Fe–Fe distance known in a Fe_4S_4 cubane-type cluster. This situation is approached in **10**. It is, therefore, highly probable that the single

(44) Laskowski, E. J.; Frankel, R. B.; Gillum, W. O.; Papaefthymiou, G. C.; Renaud, J.; Ibers, J. A.; Holm, R. H. *J. Am. Chem. Soc.* **1978**, *100*, 5322.
(45) Carney, M. J.; Whitener, M. A.; Papaefthymiou, G. C.; Frankel, R. B.; Spartalian, K.; Holm, R. H. *Inorg. Chem.* **1988**, *27*, 346.
(46) Nelson, L. L.; Lo, F. Y.-K.; Rae, A. D.; Dahl, L. F. *J. Organomet. Chem.* **1982**, *225*, 309.
(47) Excluding species with $Fe(RNC)_{5,6}$ stoichiometries, this situation is approached only in the reaction product of $Fe(t\text{-BuNC})_5$ and MeI: Bassett, J.-M.; Green, M.; Howard, J. A. K.; Stone, F. G. A. *J. Chem. Soc., Dalton Trans.* **1980**, 1779.
(48) (a) Pelizzi, G.; Albertin, G.; Bordignon, E.; Orio, A. A.; Calogero, S. *Acta Crystallogr.* **1977**, *B33*, 3761. (b) Drew, M. G. B.; Dodd, G. H.; Williamson, J. M.; Willey, G. R. *J. Organomet. Chem.* **1986**, *314*, 163. (c) Constant, G.; Daran, J.-C.; Jeannin, Y. *J. Inorg. Nucl. Chem.* **1973**, *35*, 4083. (d) Schaal, M.; Weigand, W.; Nagel, U.; Beck, W. *Chem. Ber.* **1985**, *118*, 2186.
(49) Albertin, G.; Orio, A. A.; Calogero, S.; Di Sipio, L.; Pelizzi, G. *Acta Crystallogr.* **1976**, *B32*, 3023.

diamagnetic Fe(II) subsite in clusters **5–9** is separated by ca. 3.2 Å from the Fe atoms of the spin-isolated Fe_3S_4 fragment.

Redox Reactions and Possible Biological Implications. The cyclic voltammograms of clusters **3** and **7** in dichloromethane, presented in Figure 10, reveal the chemically reversible series 9 and 10 (R = *t*-Bu) involving *two* core oxidation-state changes,

$$[Fe_4S_4(LS_3)Cl]^{3-} \overset{-1.08}{\rightleftharpoons} [Fe_4S_4(LS_3)Cl]^{2-} \overset{+0.12}{\rightleftharpoons} [Fe_4S_4(LS_3)Cl]^{1-} \quad (9)$$

$$[Fe_4S_4(LS_3)(RNC)_3]^{2-} \overset{-1.08}{\rightleftharpoons} [Fe_4S_4(LS_3)(RNC)_3]^{1-} \overset{-0.18}{\rightleftharpoons} [Fe_4S_4(LS_3)(RNC)_3]^{0} \quad (10)$$

$[Fe_4S_4]^{3+/2+}$ and $[Fe_4S_4]^{2+/1+}$. Values of $E_{1/2}$ (V) are indicated. Coulometric oxidation of **7** at −0.10 V gave n = 1.0; rereduction at −0.30 V resulted in n = 0.80. Coulometric reduction of this cluster at −1.2 V was poorly behaved, indicating instability of the reduced form over the time (ca. 30 min) of the experiment. Usually, oxidation to the $[Fe_4S_4]^{3+}$ level is irreversible; reversible couples heretofore have been observed with clusters in hydrophobic environments, often produced by sterically bulky ligands.[50] All clusters of type **2** that we have examined in dichloromethane show these two reversible redox steps. This behavior illustrates a stabilizing feature of the LS_3 ligand system that is not displayed by halide and unhindered thiolate ligands alone or in combination.

Cluster **10** exhibits the chemically reversible process 11 in dichloromethane with the indicated $E_{1/2}$, ΔE_p = 130 mV (50 mV/s), and i_p/i_a = 1. Coulometric oxidation at +0.50 V gave

$$[Fe_4S_4Cl_2(t\text{-BuNC})_6] \overset{+0.30}{\rightleftharpoons} [Fe_4S_4Cl_2(t\text{-BuNC})_6]^{1+} \quad (11)$$

n = 1.0 and a color change from purple to brown. Reduction of this solution at 0.10 V resulted in n = 0.93 and restoration of the dark purple color of the solution. A poorly defined irreversible reduction was detected near −1.1 V.

Isonitriles and carbon monoxide are strong π-acceptors and often form analogous compounds. A significant difference between them is the tendency of isonitriles to stabilize higher oxidation states. Simple examples in Fe chemistry include $Fe(CO)_5$/$Fe(RNC)_5$,[51] the stable complexes $[Fe(RNC)_5L]^{2+,1+}$ (L = neutral or anionic ligand, or absent),[52] and the absence of $[Fe(CO)_5L]^{2+}$. This tendency is reflected in redox series 9 and 10, where the $[Fe_4S_4]^{3+}$ oxidation level is obtained at relatively low potentials in reversible reactions. The $[Fe_4S_4]^{1+}$ state is produced at the *same* potential when either **3** or **7** is reduced in dichloromethane; given the 1- charge of **7**, a less negative reduction potential might have been expected. Evidently, the charge difference is offset by σ-donation to the core by three *t*-BuNC ligands.[53] In reaction 11, the oxidized cluster presumably has Fe(III) character at the isonitrile subsites. Also consistent with relative reactivities of the two ligands is the failure of cluster **3** in acetonitrile to react with CO after prolonged bubbling at 1 atm. Similarly, $[Fe_4S_4(SPh)_4]^{2-}$ is reported to be inert to CO (1 atm) in DMA solution, but $[Fe_4S_4(SPh)_4]^{3-}$ forms (unidentified) CO species that are EPR-detectable in frozen DMA solutions.[54]

A number of ferredoxin-dependent enzymes or enzymes containing Fe–S clusters are inhibited competitively or in a dead-end fashion by carbon monoxide. For example, CO is a potent inhibitor of all [Fe]-hydrogenases.[55] The FeMo protein of nitrogenase[56] interacts with CO, and the N_2-reducing activity of the enzyme complex is noncompetitively inhibited. On the other hand, methylisonitrile is a substrate of the enzyme.[57] One reasonable proposition derived from the present work and other observations[54-56] is that, if Fe_4S_4 clusters are involved in the inhibition process, their reaction with CO may generate a species such as $[Fe_4S_4(S\text{-}Cys)_3(CO)_3]^{2-}$. The reactive subsite in the $[Fe_4S_4]^{1+}$ core would be rendered low-spin Fe(II) in the process of forming the stable $Fe(CO)_3$ group. The extent to which this group would influence the native cluster properties of redox potential and charge distribution remains to be determined, as does the influence of isonitrile binding on such properties. We are currently examining the reactions of CO with clusters of type **2** in the 3+ and 1+ core oxidation levels. We note that active aconitase,[4] with labile aquo or hydroxo ligands at its unique subsite,[22] is a promising case for examination of the effects of RNC and CO binding on the properties of a native Fe_4S_4 cluster.

Acknowledgment. This research was supported by NIH Grant GM 28856 at Harvard University and by NIH Grants GM 22701 (E.M.) and GM 32394 (E.P.D.) at the University of Minnesota. X-ray equipment was obtained through NIH Grant 1 S10 RR 02247. We thank Dr. M. Carrié, Dr. K. K. Surerus, and S. C. Lee for experimental assistance and useful discussions, and Dr. G. C. Papaefthymiou for the use of Mössbauer equipment.

Supplementary Material Available: For $[Fe_4S_4Cl_2(t\text{-BuNC})_6]$, crystallographic data, tables of intensity collection and structure refinement parameters, positional parameters, and anisotropic and isotropic temperature factors (4 pages); calculated and observed structure factors (31 pages). Ordering information is given on any current masthead page.

(50) (a) Mascharak, P. K.; Hagen, K. S.; Spence, J. T.; Holm, R. H. *Inorg. Chim. Acta* **1983**, *80*, 157. (b) O'Sullivan, T.; Millar, M. M. *J. Am. Chem. Soc.* **1985**, *107*, 4096. (c) Pickett, C. J. *J. Chem. Soc., Chem. Commun.* **1985**, 323. (d) Okuno, Y.; Uoto, K.; Yonemitsu, O.; Tomohiro, T. *J. Chem. Soc., Chem. Commun.* **1987**, 1018. (e) Nakamoto, M.; Tanaka, K.; Tanaka, T. *J. Chem. Soc., Chem. Commun.* **1988**, 1422. (f) Ohno, R.; Ueyama, N.; Nakamura, A. *Chem. Lett.* **1989**, 399.

(51) Bassett, J.-M.; Berry, D. E.; Barker, G. K.; Green, M.; Howard, J. A. K.; Stone, F. G. A.; Wolsey, W. C. *J. Chem. Soc., Dalton Trans.* **1979**, 1003.

(52) (a) Bonati, F.; Minghetti, G. *J. Organomet. Chem.* **1970**, *22*, 195. (b) Bonati, F.; Minghetti, G.; Leoni, R. *J. Organomet. Chem.* **1970**, *25*, 223.

(53) We have made analogous observations elsewhere.[6]

(54) Averill, B. A.; Orme-Johnson, W. H. *J. Am. Chem. Soc.* **1978**, *100*, 5234.

(55) (a) Adams, M. W. W.; Mortenson, L. E. *Biochim. Biophys. Acta* **1981**, *594*, 105. (b) Adams, M. W. W. *Biochim. Biophys. Acta*, in press.

(56) (a) Davis, L. C.; Henzl, M. T.; Burris, R. H.; Orme-Johnson, W. H. *Biochemistry* **1979**, *18*, 4860. (b) Lowe, D. J.; Eady, R. R.; Thorneley, R. N. F. *Biochem. J.* **1978**, *173*, 277.

(57) Rubinson, J. F.; Corbin, J. L.; Burgess, B. K. *Biochemistry* **1983**, *22*, 6260.